Electrical Impedance Tomography: Tissue Properties to Image Measures

Andy Adler, Alistair Boyle

***Abstract*—Electrical Impedance Tomography (EIT) uses electrical stimulation and measurement at the body surface to image the electrical properties of internal tissues. It has the advantage of non-invasiveness and high temporal resolution but suffers from poor spatial resolution and sensitivity to electrode movement and contact quality. EIT can be useful to applications where there are conductive contrasts between tissues, fluids or gasses, such as imaging of cancerous or ischemic tissue or functional monitoring of breathing, blood flow, gastric motility and neural activity. The past decade has seen clinical application and commercial activity using EIT for ventilation monitoring. Interpretation of EIT-based measures is complex, and this review paper focuses on describing the image interpretation "pathway." We review this pathway, from *Tissue Electrical Properties*, *EIT Electrodes & Hardware*, *Sensitivity*, *Image Reconstruction*, *Image Processing* to *EIT Measures*. The relationship is discussed between the clinically-relevant parameters and the reconstructed properties. An overview is given of areas of EIT application and of our perspectives for research and development.**

I. Introduction

Electrical Impedance Tomography (EIT) is a technique to image the electrical properties within a body using electrical stimulations and measurements applied at electrodes on the body surface. EIT is useful when the anatomical or physiological phenomena of interest create contrasts in the tissue electrical properties. Examples of anatomical contrasts are the altered electrical impedance spectra of cancerous [63] and ischemic [81] tissues. Functional contrasts are created by changes in the conductivity of tissue or the movement of conductively contrasting fluids or gasses, such as during breathing, blood flow, digestive or nervous activity.

As a medical imaging modality, EIT offers several advantages: the non-invasive attachment to a patient with electrodes and wires is convenient for continuous monitoring applications; it does not use ionizing radiation; it is capable of functioning at high frame rates giving good temporal resolution; it is potentially inexpensive, using off-the-shelf low-frequency electronics components. On the other hand, EIT has poor spatial resolution, and is prone to artefacts from electrode movement and poor contact quality.

Medical interest in EIT began in the late 1970s [54] and early 1980s [15], and focussed on thoracic imaging, with a subsequent interest in imaging the abdomen, brain, and breast. Mathematical interest began in 1980 [27] proving the existence and uniqueness of the reconstructed EIT solution under a variety of assumptions [100]. Subsequent work in the mathematical community has connected EIT to the broader field of inverse problems [104]. Commercial interest in EIT has varied over time. In the 1990s and 2000s the systems developed by research groups were made available commercially. In the last decade, commercial devices have been refined to meet the requirements of clinical use, and EIT is beginning to be used clinically for adult and pediatric ventilation monitoring [42]. The progression of interest can be seen in the publications rate on EIT [7], which shows a sharp increase after 2000.

The concepts behind EIT were invented in the geophysical community in 1911 [12], where the technique is called electrical resistivity tomography (ERT). ERT can image conductive (i.e. metal-bearing) ore and the presence and movement of liquids (e.g. for groundwater and leaching). This technology (and the related electrical capacitance tomography, ECT) has also been used in industrial applications, for imaging the flow and mixing of industrial fluids (process tomography) [17], and as pressure sensitive skin for robotics applications [94].

A brief note on terminology: EIT is named for "impedance" even though the volumetric property which is imaged is the impedivity or resistivity (or the inverse, admittivity or conductivity) [16]. This terminology follows the convention that tomographic modalities are named after the source measurements; EIT uses multi-port impedance measurements from which a tomographic image is calculated.

Numerous review articles have been published on various aspects of EIT. These include general overviews [26], [58], [29], reviews focusing on the mathematical (inverse problem) aspects [10], [19], [104], and general reviews of EIT's clinical applications [36]. Several reviews of the thoracic applications of EIT have been written, focusing primarily on the monitoring of ventilation [7], [18], [33], [42], [41], [38], [74], [88] with some recent reviews on monitoring of blood perfusion [67], [79]. This review paper is designed to contribute a novel viewpoint to this literature, focusing on the connections between the aspects of image interpretation – from tissue properties, through EIT hardware, the forward and inverse problems to the EIT measures relevant to clinical interpretation.

A. Modalities of EIT

Applications of EIT can be classified between those for providing images and for functional monitoring. As an *imaging modality*, EIT estimates an anatomical image of the distribution of conductivity. A reconstruction at a given time from a single set of measurements is called absolute EIT (aEIT). Unfortunately, aEIT has proved to be very sensitive to errors

AA is with Systems and Computer Engineering, Carleton University, Ottawa, AB is with Electrical Engineering and Computer Science, University of Ottawa

TABLE I: EIT Applications

Application	*Description*
Lung function	- Distribution of tidal volume [52] - Regions of overdistension, atelectasis [46], [34] - Recruitment/derecruitment of lung tissue [40] - Respiratory system mechanics [86] - Regional compliance ($\Delta Z/\Delta P$) - Opening and closing pressures [85] - Edema and extra-vascular lung water [102] - Alarms: one-lung ventilation, pneumothorax
Perfusion & cardiac function	- Regional Distribution of blood flow [95] - Contrast-based perfusion measurement [39] - Pulsatility-based perfusion measurement [95] - Cardiac output - Systemic blood pressure (via pulse timing) [96] - Pulmonary blood pressure (via pulse timing) [84] - Intravascular fluid responsiveness [103] - Ventilation-perfusion matching
Neural & brain activity	- Stroke (Hemorrhagic vs. Ischemic)† [89] - Epileptic regions and foci† - Cerebral perfusion [5] - Neural activation (via opening of ion channels) [13] - Cerebral activation pattern for evoked potentials - Cerebral edema [57]
Cancerous tissue	- Breast cancer screening† [14], [31] - Prostate cancer screening† [21], [51] - EIT + mammography† [32] - EIT + ultrasound† [97]
Other	- Gastric and Intestinal motility [76] - Pharyngeal transit times [76] - Bladder volume and emptying [66] - Edema† [1], [78] - Hemorrhage and blood accumulation† [91]

†*indicates use of aEIT or fdEIT imaging; others use tdEIT*

such as inaccuracies in the assumed model geometry, and non-ideal properties of electrodes and amplifiers [8], [80]. Another approach to anatomical imaging is frequency-difference EIT (fdEIT) in which measurements at two or more excitation frequencies are used to calculate an image of the difference in electrical properties between the frequencies.

As a *functional monitoring* technology, EIT is sensitive to changes in tissue properties over time. Time-difference (tdEIT) image reconstruction, is more stable since it is less sensitive to interferences which remain stable [26]. The main application of tdEIT has been for breathing (moving non-conductive air) and heart activity (moving conductive blood).

B. Applications of EIT

Many medical applications have been proposed for EIT, and an overview is shown in table I, including some early references for each use. Those based on imaging (using aEIT or fdEIT) are indicated with †, while the others use tdEIT. For a detailed review of thoracic applications of EIT, see [42] and for other applications see [58].

Imaging applications of EIT have primarily focused on detection and localization of pathologies: cancerous tissue (in the breast [14], [31] and prostate [21]) where the electrical properties of cancerous tissue differ from benign [63]; ischemic tissue (as seen in stroke) where electrical properties vary with ionic concentrations [57]; and hemorrhage and blood pooling (characterized by the presence of conductive blood).

The main monitoring application of EIT is for monitoring of breathing and blood flow [42]. For mechanical ventilation, there are dangers to both too much and too little support pressure, and EIT shows potential to guide a patient-specific level of support [110]. For obstructive lung diseases, such as chronic obstructive pulmonary disease (COPD) and asthma, lung heterogeneity is not measured by current diagnostic tools, and EIT shows an increased diagnostic sensitivity [105]. EIT can measure heart and blood-flow parameters, including cardiac output [106], pulmonary perfusion [39], systemic [96] and pulmonary arterial [84] pressure.

Many other monitoring applications of EIT are promising. Neural and brain activity have been imaged, where the opening of ion channels during neural action produces a conductivity change [13]. Gastric motility and pharyngeal transit times can be measured by EIT [76]. Other applications include the fluid volume of the bladder [66], accumulation of edema in the lungs [78] brain or peripheral tissue [1], and hemorrhage and blood pooling [91].

II. EIT IMAGE GENERATION AND INTERPRETATION

This review focuses on clarifying the various processes between tissue electrical properties and diagnostic EIT measures, in order to help clarify interpretation of EIT results. This *image interpretation pathway* (fig. 1, modified from [42]) categorizes the "steps" by which an EIT system creates measures of the tissue properties of interest. Subsequent subsections address each step in the process.

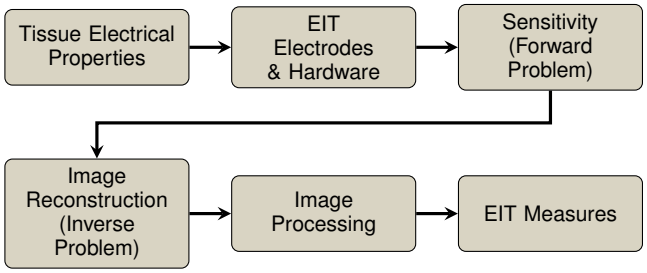

Fig. 1: Image interpretation pathway, by which diagnostically-relevant measures are created from the electrical properties of tissues

A. Tissue Electrical Properties

In general, the electrical properties of tissues themselves are not of immediate medical interest. Instead, the relationship between contrasting electrical properties reflect physiological or anatomical changes of interest. For sinusiodal current excitation at frequency $\omega = 2\pi f$, tissue can be modeled by a complex conductivity $\sigma^* = \sigma + j\omega\epsilon_r\epsilon_0$, with ohmic conductivity σ and permittivity, $\epsilon_r\epsilon_0$. Biological tissues have a complicated relationship between σ^* and f. Through most frequency ranges, σ^* increases monotonically with f (characterized by a single time constant), but the curve is interspersed with a sequence of plateaus called dielectric dispersions [43]. Biological materials have high dielectric constants compared to homogeneous materials due to biological membrane surfaces and macromolecules. For example, cancerous breast tissue shows a different conductivity spectrum from non-malignant tissues [63], where the effects were explained as

a result of the increased density of tumor stroma. Differences in the σ^* spectrum between tissue types is the source of contrasts in fdEIT images. Some tissues, such as skin, muscle and deflated lung, display properties with identifiable low-frequency charateristics [44]. Unfortunately, much of the interesting tissue electrical properties occur in the MHz range, as current begins to flow accross the cell membranes, but MHz stimulation is above the maximum operating frequency of most EIT systems.

For functional EIT imaging, the changes in tissue electrical properties are caused by the movement of conductive fluids and non-conductive gasses into the tissue. Fortuitously, the relationship between change in alveolar air content and increase in resistivity has been found to be linear, both experimentally, and via constitutive models [90]. This has allowed interpretation of the air content in tdEIT lung images via a simple calibration factor. On the other hand, the relationship between cardiac activity and electrical properties is far more complicated. The conductivity of blood is higher than most other tissues, but varies with the orientation of the red blood cells and the speed of flow [56]. tdEIT is only sensitive to the pulsatile component of flow and not to constant flows [42]. Finally, the motion of the heart in the chest cavity creates large contrasts in EIT images [83].

Chemical and pH changes in tissue, such as those due to muscular fatigue and ischemia, change σ^* [81]. Neural and muscular tissue also have electrical properties which change when active. For low-frequency electrical stimulation, the opening of ion channels in cellular membranes [13] creates conductivity contrasts.

Many biological tissues have anisotropic electrical properties, such as muscles and nerves, where the conductivity is larger in the fibre direction. This anisotropy makes the relationship between tissue electrical properties and EIT images non-unique [69], although it may be possible to apply additional constraints for anisotropic tissue during image reconstruction to yield useful results [71].

B. EIT Electrodes & Measurement Electronics

EIT normally makes measurements at electrodes on the body surface (although internal electrodes have been proposed in the esophagus [92] and for prostate imaging [21]). For ease of application, electrodes are sometimes incorporated into a belt or harness [108], but are also applied individually. Both non-polarizable (ECG-type Ag/AgCl electrodes) and polarizable (stainless steel, conductive fabrics and rubbers) have been used. When operating at stimulation frequencies in the kHz range (as do most systems), the polarization of electrodes is a less significant effect.

Electrical current levels are limited by electrical safety considerations. The relevant standard is the "patient auxiliary current" defined by IEC 60601-1 [60], which has been interpreted as limiting the maximum total stimulation current into the body over all electrodes. This current is limited to $100\,\mu\mathrm{A}$ at low frequency and increases with frequency to a maximum of $10\,\mathrm{mA}$ at $100\,\mathrm{kHz}$. Most recent EIT systems use a stimulation frequency near to or above $100\,\mathrm{kHz}$ in order to maximize injected current and thus signal to noise ratio. Internal electrodes [92] (especially in the esophagus, as it is near the heart) would need to meet much stricter stimulation and leakage current limits.

EIT is especially sensitive to changes at or near the electrodes where the current density is highest. Two main changes are of concern: movement of electrodes, and changes in contact quality. Electrodes move during breathing and with changes in posture, which introduces artefacts [2]. Ensuring a good electrode connection to the skin is vital to the quality of EIT data. Many gels and liquids appear to improve contact quality [108]; however, data quality may decrease in prolonged measurements as electrodes dry [73]. Electrode contact quality can also vary with posture changes [35] and the change in the pressure applied to electrodes.

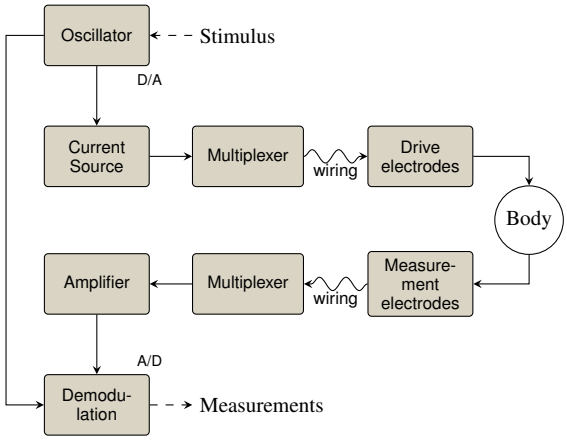

Fig. 2: Block diagram of pair-drive EIT system. A sinusiodal waveform is created by a stable oscillator, which drives a current source with a high impedance output. This current is multiplexed onto the chosen electrode pair. On the body, the measurement electrodes are connected to an instrumentation amplifier with high common-mode rejection ratio (CMRR). The amplified output is demodulated and converted to a digital value which can be further processed.

EIT systems typically apply sinusiodal currents to the body and make voltage measurements. The most common configuration is pair-drive, in which current is applied across one pair of electrodes while the voltage across all other pairs of electrodes is measured (fig. 2). Early systems used analog demodulation, while most modern systems demodulate the digitized signal numerically.

Since the pair-drive configuration is so common, it is worth describing these systems in more detail. The term "stimulation and measurement pattern" refers to the sequence of electrodes to which currents are applied and voltages measured. The earliest systems used an adjacent or "Sheffield" protocol, illustrated in fig. 3. Unfortunately, the adjacent pattern has very poor sensitivity to internal changes [6] (fig. 6), so many recent systems use pair drive with a "skip" distance between the driven and measurement electrodes.

A number of alternatives to the serialized, pair-drive configuration have been used. First, several systems make simultaneous parallel measurements, which can be faster. The waveform is most commonly sinusoidal (using an oscillator, or more recently, digital synthesis) or approximated with a square

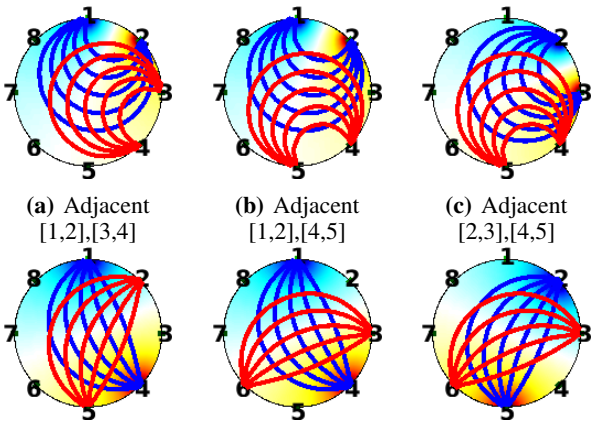

(a) Adjacent [1,2],[3,4] **(b)** Adjacent [1,2],[4,5] **(c)** Adjacent [2,3],[4,5]

(d) Skip 2 [1,4],[2,5] **(e)** Skip 2 [1,4],[3,6] **(f)** Skip 2 [2,5],[3,6]

Fig. 3: Illustration of pair-drive stimulation and measurement patterns for an 8 electrode system using (top row) an adjacent pattern, and (bottom row) a "skip 2" pattern. Background colours indicate electrical potential (red positive through blue negative) due to stimulus electrodes. Stream lines indicate the stimulus current flow (blue lines) and measurement current flow if measurement electrodes were used as stimulus (red lines). The dot product of the stimulus and measurement current flows in a region gives the sensitivity of the measurements to a change in conductivity within that region.

wave. A set of "optimal current patterns" have been defined [61], which require the simultaneous current stimulation and voltage measurement accross all electrodes [59]. Such capability can also be used to simultanously drive all electrodes at different frequencies in order to avoid multiplexing [87]. To reduce interference, active electrodes have been designed and placed near or within the electrodes [68], in order to reduce interference onto the weak measured signals. Finally, some systems stimulate the body with an applied voltage rather than an applied current [64] which is technically simpler, but more sensitive to the contact impedance.

In order to achieve good performance from an EIT system, there are several challenges to overcome. The dynamic range of measured signals is high because voltages are much larger near driven electrodes; systems thus require either a high A/D converter resolution, or adjustable channel gain. When considering the electrical characteristics of the electrode contact with the skin, there are two relevant parameters both of which have unfortunately been called "contact impedance". The electrode-body contact impedance ($Z_{\mathrm{C,EB}}$) represents the resistance to be overcome by the EIT current source, while the electrode-surface contact impedance ($Z_{C,ES}$) characterizes the electrode material, and allows an external pathway for current which would normally flow in the body (see fig. 4). A complete model of the EIT system would also account for the electrode connections, $Z_{\mathrm{C,EB}}$, and for the wiring or amplifier characteristics [53].

Common-mode voltages are high when $Z_{\mathrm{C,EB}}$ is not equal across the drive electrode pair, and high CMRR is required. Additionally, high amplifier output impedance, $\mathrm{Z_{out}}$, is required so that the driven current does not vary with $Z_{\mathrm{C,EB}}$. While many designs have claimed very high CMRR and $\mathrm{Z_{out}}$, these values represent DC amplifier specifications; most IC amplifiers have much worse performance at 100 kHz and above. The inductive coupling between the electrode leads and capacitive coupling to the body allow interference and crosstalk between electrode channels. Polarization of electrodes is less significant at the high frequencies used in medical EIT, but it is important to ensure that complete current cycles are used for each measurement, otherwise a net DC current can be passed to the body. Finally, the signal to noise ratio is limited by the number of cycles. For example, a serial 32 electrode system operating at 50 frames/s must make $50 \times 32^2 \approx 50\,000$ acquisitions/s. At a stimulation current of 100 kHz, only one cycle can be measured, since the first will be lost to the switching transients of the multiplexers.

C. Sensitivity (Forward Problem)

For a given conductivity distribution within the body, the prediction of measured values, $\mathbf{v}$, is the "forward problem", which also includes analysis of the sensitivity of $\mathbf{v}$ to changes in conductivity [29]. Using N_E electrodes, an EIT system calculates a *frame* of N_M data measurements, $\mathbf{v} \in \mathbb{C}^{N_m}$. Using pair-drive and avoiding measurements on the driven electrodes, $N_M = N_E(N_E - 3)$. The maximum number of independent measurements possible on N_E electrodes is $\frac{1}{2}N_E(N_E - 1)$, due to reciprocity (i.e. the sensitivity is unchanged if drive and measurements are interchanged). In the EIT literature, the reciprocity principle is commonly cited as [45], although it was known much much earlier [72]. Measurements, $\mathbf{v}$, can have complex values indicating the in- and out of-phase components, although it is common to only consider the in-phase component, which dominates at low frequencies.

The current density, $\vec{J}$, and electric field, $\vec{E}$, in the body are related by Ohm's law, $\vec{J} = \sigma\vec{E}$, where $\sigma(\vec{x}, t)$ is the tissue conductivity and may vary in space and time. Since $\vec{E}$ varies sinusoidally with the drive current, it can be represented as a phasor and a complex conductivity σ^* at the drive frequency. In anisotropic tissue, σ^* is a symmetric tensor. Continuity requires $\nabla \cdot \vec{J} = \frac{\partial}{\partial t}\rho$, but since charge does not accumulate in a conductor, the charge density, $\rho = 0$. The quasi-static approximation assumes that the time derivative of the magnetic field is negligible, $\nabla \times \vec{E} = -\frac{\partial}{\partial t}\vec{B} \approx 0$, and is valid when the length scales of interest are much smaller than the electromagnetic wavelength [65]. In this case, the electric field can be described by a voltage, V, where $\vec{E} = -\nabla V$, and the voltage distribution in the body is determined by Laplace's (or Poisson's) equation

$$\nabla \cdot \sigma \nabla V = 0. \tag{1}$$

The boundary conditions specify the normal current, J_n, at the electrodes, depending on the drive pattern, and require that current be zero where there are no electrodes. Since absolute voltage is arbitrary, a reference voltage must be specified at a point, either at a ground electrode or at an internal point. At a drive electrode, current distributes through the electrode material before flowing into the body. Several models of electrode current flow have been used [29]. The simplest are the "continuum", and "gap" models which assume current flows with uniform magnitude across each electrode.

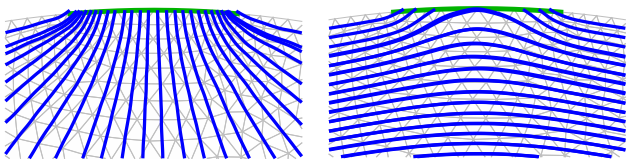

(a) Drive electrode **(b)** Measurement electrode

Fig. 4: Current streamlines near drive and measurement electrodes, with $Z_{C,ES} = 0.01\,\Omega \cdot \mathrm{m}$, $\sigma = 1\,\Omega^{-1}\mathrm{m}$. When the impedance of the electrode material is significantly lower than the body, current can take a "short-cut" through a measurement electrode and tends to have highest density near the edges of drive electrodes.

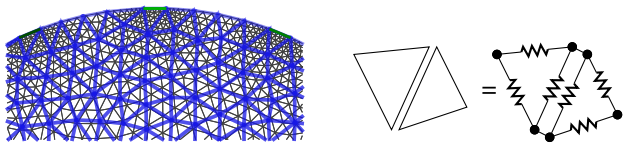

(a) Dual FEM mesh **(b)** First-order FEM as a resistor mesh

Fig. 5: Illustration of a 2D FEM discretization of the forward model (left, black). Meshing is refined near electrodes to better model large gradients. The reconstruction model mesh (left, blue) is related to the FEM by $\mathbf{M}$. First order triangular elements are equivalent to a resistor mesh (right) with conductance $Y_{i,j} = \sigma_i \cot \alpha_{i,j}$.

If electrode shapes vary, the gap model divides applied current over the electrode area. However, when electrodes are more conductive than the body, current flows preferentially through the electrode material and current density is highest at the electrode edges. For very conductive electrode material, the "shunt" model assumes a constant voltage across each electrode, while the "complete electrode model" (CEM) accounts for the electrical properties of the electrode material, $Z_{C,ES}$ [30], and is used by most recent work. Fig. 4 shows the current propagation in the region of a drive and measurement electrode.

An analytic solution of (1) is only available for regular geometries and their conformal deformations. For realistic geometries, numerical techniques are required. The finite element method (FEM) has been the approach of choice, because it allows numerical refinement in regions of high $\vec{J}$, such as near the electrodes [48]. The EIT community has traditionally used linear first-order FEM models, as these have been sufficient given the accuracy with which the body shape is known [47]. Using a FEM model, the body is discretized into N_F elements, where the conductivity of each is represented by a vector $\boldsymbol{\sigma}_F \in \mathbb{C}^{N_F}$. For calculation of the sensitivity, the discretization may be different than the FEM mesh for the forward solution (fig. 5), for example using a voxel representation. Representing the sensitivity as $\boldsymbol{\sigma} \in \mathbb{C}^{N_S}$, we calculate $\boldsymbol{\sigma} = \mathbf{M}\boldsymbol{\sigma}_F$, where $\mathbf{M}_{i,j}$ represents the volume fraction of forward element j in sensitivity element i.

For a uniform notation, we define the *measured data*, $\mathbf{y}$. For aEIT, $\mathbf{y} = \mathbf{v}$, and for difference EIT, $\mathbf{y} = \mathbf{v} - \mathbf{v}_r$, as it reconstructs the changes between the measurement of interest, $\mathbf{v}$, and a reference $\mathbf{v}_r$, For normalized difference EIT, $\mathbf{y} = (\mathbf{v} - \mathbf{v}_r)./\mathbf{v}_r$ where $\cdot./\cdot$ is the element-wise (Hadamard) division operator. Algorithms for fdEIT are based on difference imaging, in which $\mathbf{v}$ is the measurements at the stimulation frequency of interest and $\mathbf{v}_r$ the measurements at the reference frequency. These algorithms requre data to be scaled appropriately, using a k such that $\mathbf{y} = \mathbf{v} - k\mathbf{v}_r$ [93].

The image parameters of interest are defined as $\mathbf{x} = \boldsymbol{\sigma}$ for aEIT and $\mathbf{x} = \boldsymbol{\sigma} - \boldsymbol{\sigma}_r$ for difference EIT. Various algorithms parameterize $\mathbf{x}$ differently depending on specific requirements. The FEM-based forward calculation is thus

$$\mathbf{y} = F(\mathbf{x})|_{\boldsymbol{\sigma}=\boldsymbol{\sigma}_r}\,, \tag{2}$$

where, for difference EIT, $\mathbf{v}_r$ is calculated at an assumed "background conductivity", $\boldsymbol{\sigma}_r$.

The Jacobian, $\mathbf{J}$, or sensitivity matrix, represents the sensitivity of each measurement to a conductivity change in each image region,

$$\mathbf{J}_{i,j} = \frac{\partial}{\partial \boldsymbol{\sigma}_j} F(\mathbf{x})_i \bigg|_{\boldsymbol{\sigma}=\boldsymbol{\sigma}_r}. \tag{3}$$

Two approaches to calculation of $\mathbf{J}$ have been used: direct differentiation of the FEM system matrix formulation [111], and adjoint field methods [82], in which the dot (inner) product of fields produced by stimulation and measurement patterns are integrated over each image element. The first requires a custom FEM solver, while the later technique can accept the output of standard FEM algorithms. An efficient implementation of both methods results in the same underlying algorithm [11]. It is also possible to approximate $\mathbf{J}$ by making small changes in each image region, and calculate a "perturbation Jacobian" [111]. Efficient calculation of both the forward solution and Jacobian are important to the performance of EIT solvers [23]. The perturbation approach is generally slower to execute but easiest to implement making it suitable for validating alternate implementations.

The matrix $\mathbf{J}$ may be used to investigate aspects of an EIT system configuration. Each column represents the change in measurements, $\partial\mathbf{v}$, due to a conductivity contrast in the corresponding FEM element, while each row represents the relative contribution to each FEM element from the corresponding measurement. To visualize sensitivity patterns, the contribution from each FEM element, i, should be normalized by the element size (volume, V_i); thus, the sensitivity, S_i, of EIT data to conductivity changes in each element i is $S_i = (V_i)^{-1}(\sum_j J_{i,j}^2)^{\frac{1}{2}}$.

While the sensitivity patterns of EIT are well understood for single-plane electrode placements, EIT is inherently sensitive to off-plane conductivity contrasts (fig. 7), showing a "lens-shaped" sensitivity region. By using a vertical placement of electrodes, it is possible to constrain the region of sensitivity [50]. EIT may also be used to create 3D images [77], although the reconstructions are unreliable in regions far from electrodes as the sensitivity is very small.

While sensitivity for conductivity changes is equal for small conductive and non-conductive contrasts, the sensitivity saturates as the magnitude of the conductivity contrast increases. Fig. 8 shows the normalized sensitivity for a cylindrical ROI in a phantom with single electrode plane, as a function of shape and conductivity. EIT is generally more sensitive to

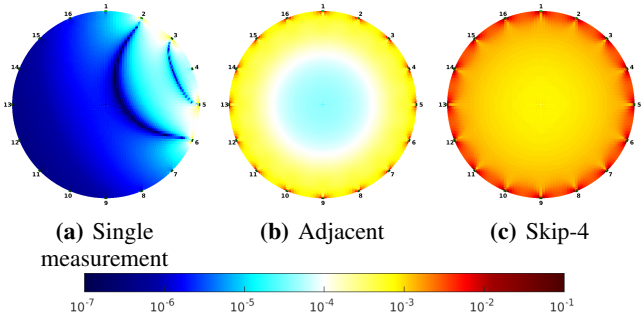

Fig. 6: Spatial distributions of EIT sensitivity for various stimulation and measurement patterns: (a) sensitivity to pair-drive measurement between electrodes [2,6],[3,5], (b) sensitivity to adjacent pattern (c) sensitivity to a "skip 4" pattern

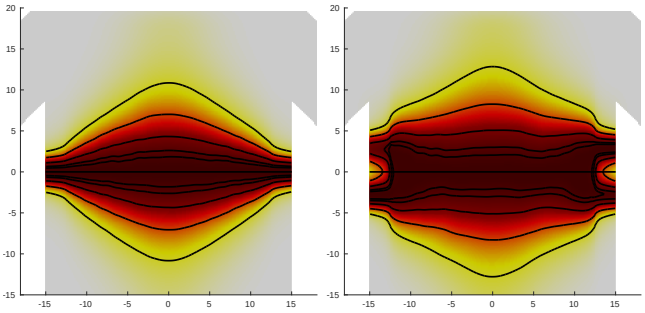

Fig. 7: Off-plane sensitivity for a cross section through an elliptical model of a uniform thorax, for (left) single 32-electrode plane (skip 5), and (right) two 16-electrodes planes (skip 5 square pattern). The relative sensitivity of each vertical pixel is calculated with respect to the on-plane value, and shown by the contours (indicating 95%, 90%, 75%, 50% and 25% of the maximum).

conductive than non-conductive contrasts, and this increased sensitivity depends on the shape; a conductive ROI lying in the path of current flow shows increased sensitivity. For spherical regions, conductive contrasts have approximately three times the sensitivity of non-conductive ones [9].

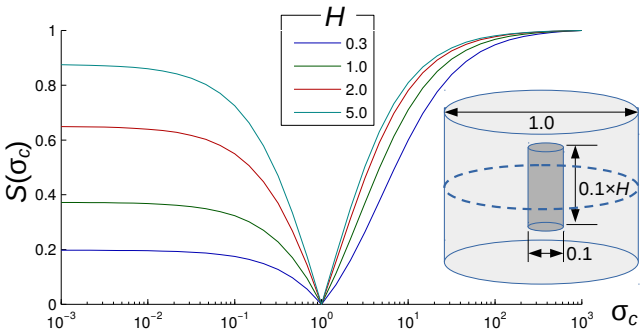

Fig. 8: The relative EIT sensitivity as a function of the shape and conductivity of a ROI. The stimulation configuration (subfigure at right) has 16 electrodes in a central plane (dotted), and a has a contrasting cylindrical ROI with a height/diameter, H, and conductivity σ_c while elsewhere $\sigma = 1$. The graph shows the normalized EIT signal, $S(\sigma_c)$, as a function of σ_c for four values of H.

D. Image Reconstruction (Inverse Problem)

Image reconstruction is an inverse problem which calculates an estimate, $\hat{\mathbf{x}}$, of the distribution of internal properties, $\mathbf{x}$, which is most consistent with the measurements, $\mathbf{y}$, and is "reasonable" in some sense (e.g. smoothness). Image reconstruction can be understood as an "inverse sensitivity" process. It is poorly conditioned, since EIT is much more sensitive to contrasts near the electrodes than in the body center. In most cases, reconstruction is also ill-posed, because the parameter space of $\mathbf{x}$ is larger than the acquired measurements, $\mathbf{y}$.

1) Regularized Image Reconstruction: The most common approach is based on minimization of a norm

$$\|\mathbf{y} - F(\hat{\mathbf{x}})\|^2_{\mathbf{W}} + \lambda^2 \|\hat{\mathbf{x}} - \mathbf{x}^*\|^2_{\mathbf{Q}}, \tag{4}$$

where the first term $\mathbf{y} - F(\hat{\mathbf{x}})$ is the "data mismatch" between the measured data and their estimate via the forward model. $\mathbf{W}$ is a data weighting matrix, and represents the inverse covariance of measurements. In most cases, $\mathbf{W}$ is set to be the identity matrix; however, given a knowledge of the reliability of each measurement channel, $\mathbf{W}$ can be used to represent this reliability during reconstruction [75]. The second term is the mismatch between the reconstruction estimate, $\hat{\mathbf{x}}$, and an *a priori* estimate of its value, $\mathbf{x}^*$. For aEIT, accurate estimation of this value is important for convergence. For difference EIT, $\mathbf{x}^* = 0$, since increases and decreases are equally likely. $\mathbf{Q}$ is the "regularization matrix" discussed later. The relative weighting between the data and prior mismatch terms is controlled by a "hyperparameter", λ. When λ is large, solutions tend to be smooth and more similar to the prior; while, for small λ, solutions have higher spatial resolution, but are noisier and less well conditioned.

The reconstructed solution, $\hat{\mathbf{x}}$, minimizes (4) and is most commonly calculated via an iterative update, $\hat{\mathbf{x}}^{(k+1)} = \hat{\mathbf{x}}^{(k)} + \delta\hat{\mathbf{x}}$ starting at $\hat{\mathbf{x}}^{(0)} = \mathbf{x}^*$, using the update

$$\delta\hat{\mathbf{x}} = \left(\mathbf{J}_k^t \mathbf{W} \mathbf{J}_k + \lambda^2 \mathbf{Q}\right)^{-1} \left(\mathbf{J}_k^t \mathbf{W} \Delta\mathbf{y} - \lambda^2 \mathbf{Q} \Delta\mathbf{x}\right), \tag{5}$$

where $\mathbf{J}_k$ is the Jacobian, updated at each iteration based on $\mathbf{x}^{(k)}$, and $\Delta\mathbf{y} = \mathbf{y} - F(\mathbf{x}^{(k)})$ and $\Delta\mathbf{x} = \hat{\mathbf{x}}^{(k)} - \mathbf{x}^*$. Often, especially for tdEIT, only one iteration is required, and a precalculated reconstruction matrix, $\mathbf{R}$, can be calculated

$$\hat{\mathbf{x}} = \left(\mathbf{J}^t \mathbf{W} \mathbf{J} + \lambda^2 \mathbf{Q}\right)^{-1} \mathbf{J}^t \mathbf{W} \mathbf{y} = \mathbf{R}\mathbf{y} \tag{6}$$

which allows for fast (real-time) reconstructions via a matrix multiplication.

Alternatively, $\mathbf{R}$ may be calculated using the "Wiener filter" form, which has been used by the GREIT [4] algorithm. Here the reconstruction matrix minimizes $\mathrm{E}_w[\|\tilde{\mathbf{y}} - \mathbf{R}\tilde{\mathbf{x}}\|^2]$, where $\tilde{\mathbf{y}}$ and $\tilde{\mathbf{x}}$ correspond to the "training" measurements and targets (i.e. representing the prior distribution of contrasts and noise), and $\mathrm{E}_w[\cdot]$ is the weighted expectation operator. The reconstruction matrix which minimizes this norm is $\mathbf{R} = \mathrm{E}_w[\tilde{\mathbf{x}}\tilde{\mathbf{y}}^t](\mathrm{E}_w[\tilde{\mathbf{y}}\tilde{\mathbf{y}}^t])^{-1}$, which yields [50]

$$\mathbf{R} = \mathbf{D}\boldsymbol{\Sigma}_t \mathbf{J}^t \left(\mathbf{J}\boldsymbol{\Sigma}_t \mathbf{J}^t + \lambda^2 \boldsymbol{\Sigma}_n\right)^{-1}, \tag{7}$$

where $\mathbf{D}$ maps each training location onto a larger "desired" image region. Eqn (7) is equivalent to (6) when parameters

are selected to be the inverse covariances $\mathbf{W} = \mathbf{\Sigma}_n^{-1}$ and $\mathbf{Q} = \mathbf{\Sigma}_t^{-1}$, and $\mathbf{D} = \mathbf{I}$.

Most regularization-based algorithms use the ℓ_2 norm in (4); however, other norms provide useful possibilities [22]. An ℓ_1 norm on the data mismatch term provides "robust error norms" which are less sensitive to outliers, while an ℓ_1 norm on the image prior term (using an appropriate $\mathbf{Q}$) enforces "total variation" regularization which has less tendency to blur image regions.

2) Regularization parameter selection: The choice of regularization matrix, $\mathbf{Q}$, and its weighting, λ, control the trade off in (4) between the data and model mismatch, and thus the amount and type of noise in reconstructed images. $\mathbf{Q}$ represents the inverse of the covariance of the expected image (or training targets). The use of Tikhonov regularization implies $\mathbf{Q} = \mathbf{I}$ and assumes that targets are independent; this choice does not work well and results in overemphasis of boundary contrasts and a "speckle"-type patterns. To address the boundary overemphasis, regularization weighting based on the sensitivity of each element has often been used, setting $\mathbf{Q}$ to the diagonal elements of $\mathbf{J}^t\mathbf{J}$, and has come to be called "NOSER regularization" [28]. Reduction of image speckle requires imposing a spatial filter into $\mathbf{Q}$. In GREIT, this is done via a larger "desired" image region and spatial correlations in the covariance, $\mathbf{\Sigma}_t$. $\mathbf{Q}$ has also been designed to impose a high-pass spatial filter to penalize non-smooth image content [20] most commonly using a Laplace filter [82].

As the "hyperparameter", λ, increases, the reconstructed image is constrained to be closer to the (smooth, low-amplitude) prior model, but loses high-frequency details. λ is often chosen heuristically, but this means that comparisons between algorithms are not fair, and can be chosen in a way to hide image artefacts. Many approaches to automatically select λ are used [24], with criteria such as image noise or the balance of norms. Fig. 9 shows sample reconstructed EIT images illustrating the effect of $\mathbf{Q}$ and λ and the reconstruction norm.

3) Alternative reconstruction approaches: The regularized reconstruction approach described in the previous section is the most common technique; however, several other approaches have been used. The earliest systems used "Sheffield back-projection" [25], which is based on the concepts from CT filtered backprojection. Most experimental work prior to this decade was based on this algorithm. Another early approach used "layer stripping" [99] in which "layers" are reconstructed moving inward from the boundary. Backprojection and layer stripping are generally considered inappropriate for most biomedical applications.

One exciting mathematical development is the "d-bar" algorithm which allows single-step nonlinear reconstruction; promising results have been shown for simulation and (tdEIT) experimental data [55]. In cases where the conductivity distribution has "jump" changes, a number of powerful techniques are available, such as the monotonicity method [101] which investigates properties of the transfer impedance map.

4) Image validation: Many parameters have been proposed to measure and compare image reconstruction performance. The most basic measure is "distinguishability", which is

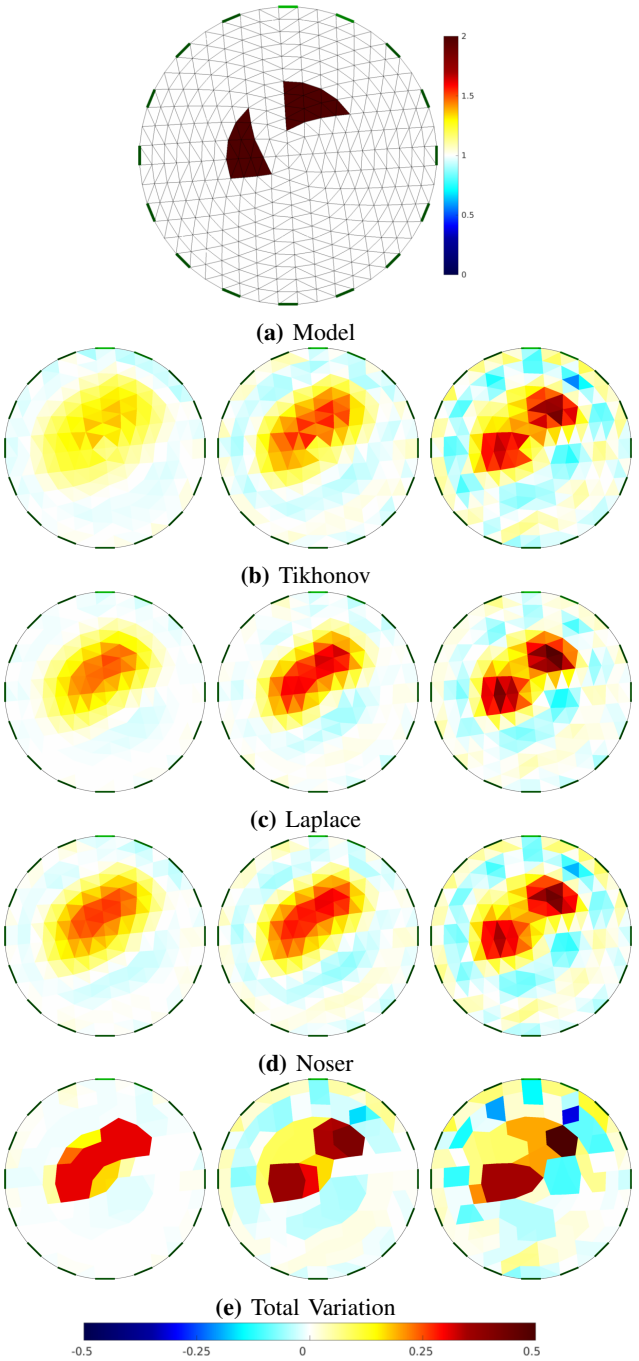

Fig. 9: EIT reconstructions as a function of hyperparameter and regularization matrix. The top row shows the simulation model from which tdEIT data are calculated, and Gaussian random noise of -12 dB SNR (reference the difference signal) added. Each row shows a different choice of prior, $\mathbf{Q}$, while the last row (Total Variation) also uses a ℓ_1 norm on the model mismatch term. Values of λ are calculated for each $\mathbf{Q}$ so that noise performance in each column is equal; noise figure values are (left column) 0.5, (center) 1.0, (right) 3.0.

related to the signal to noise ratio due to a contrast, and the probability with which such contrasts can be detected given measurement noise [62], [70]. Using simulation or phantom measurements, one can calculate the image signal to noise ratio, amplitude response, position error, resolution, ringing, and shape deformation [4]. For experimental data, images can be compared to physiological "knowns" [49]. In many cases, low-quality data (due to movement or poor contact) can be managed [75] via modifications to matrix $\mathbf{W}$. Electrode movement can be addressed to a large extent by introducing an electrode position Jacobian [98] in the reconstruction formulation.

E. Image Processing and EIT Measures

Raw EIT images do not typically give directly relevant clinical information. Instead images must be analysed to calculate application-relevant images and measures. EIT image analysis is most developed for thoracic EIT, in which a large number of functional EIT (fEIT) algorithms are available [42], fEIT approaches are classified according to the physiological parameters of interest: ventilation distribution, ventilation- and cardiac-frequency impedance changes, aeration change, respiratory system mechanics, ventilation timing, and tissue response classification.

An fEIT image is calculated from analysis of each raw image voxel over a time-sequence of EIT images to calculate a specific parameter. Examples of fEIT images are:

- *Tidal Variation*†, as a measure of the distribution of ventilation, which calculates the difference between the end-inspiratory and end-expiratory voxel values [52] (the first step of fig. 10)
- *Ventilation- or Cardiac-frequency*†, which characterize the breathing- and heart-related components of the image sequence, using a corresponding frequency filter [37], or ensemble average
- *Expiration time constant*†, as a characterization of regional lung mechanics, but fitting the expiratory part of the EIT waveform to a exponential function and reporting the exponential time constant [86]
- *Pulse propagation time*†, measuring the time for cardiac-related EIT pulses to arrive at lung voxels after the QRS peak, as a measure of pulmonary arterial pressure [84]
- *Opening- and Closing Pressures*, measuring the time delay between the start of a slow-flow inflation (deflation) and the image voxel crossing a threshold, as a measure of the pressure required to hold open lung regions [85]
- *Neural activation delay*, measuring the activation delay between neural stimulation and EIT activity in cortical regions, as a way to characterize neural pathways [13]

Some functional images († in list) are "protocol free" and can be calculated continuously as a function of time. In other cases, an intervention (lung inflation manoeuvre, neural activation, bolus injection of contrast agent [39]) are required.

EIT measures are values calculated from an image sequence which are designed to characterize tissue state. These measures are designed to represent diagnostically useful information, to determine the state of the subject and assess trends. Three types of EIT measures have been defined [42]: average measures calculate the mean fEIT image either globally, or over a ROI [37] (e.g. average tidal variation); characterizations of spatial distribution of the fEIT image (e.g. geometric center of ventilation, inhomogeneity index); and examination-specific EIT measures. The latter type can involve many steps; for example, fig. 10 shows the calculation of the hypoventilated lung fEIT measure (introduced as "silent spaces" by [107]), which represents the fraction of lung regions which receive low or no ventilation. This EIT measure is recorded as a function of time, and serves to assess the subject's state of ventilation.

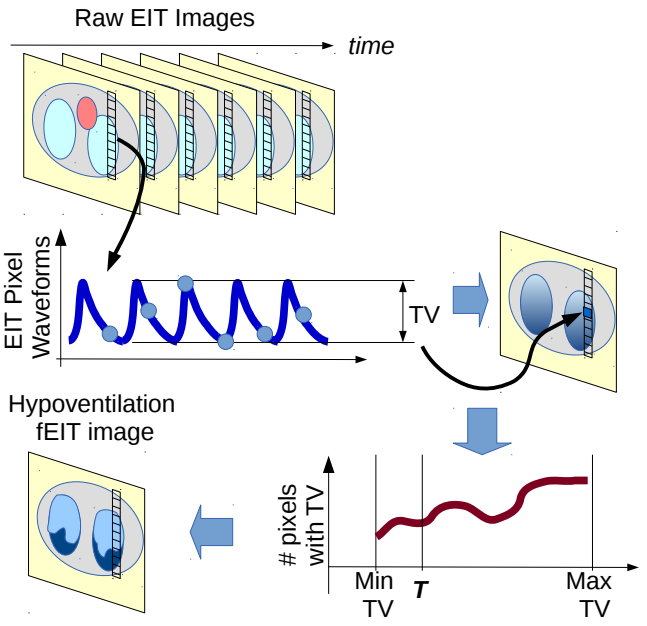

Fig. 10: Block diagram of the calculation of the fraction of hypoventilated lung [107]. From raw EIT images (top row), pixel waveforms are analyzed to calculate the tidal variation (TV) fEIT image (middle row). Within the lung ROI (identified from an anatomical atlas), regions with ventilation fraction below a threshold $T = 10\%$ are identified (bottom row) and the fraction of such pixels calculated.

For absolute imaging, EIT image processing and measures are less well developed than for tdEIT applications. Typically, the average reconstructed impedance in a region of interest is compared to a threshold. For example, cancerous prostate tissue had significantly greater conductivity than benign regions [109].

III. Discussion and Perspectives

In this review of EIT, we focus on the steps involved in interpretation of EIT images, from the electrical properties of the tissue (which by themselves are rarely of direct clinical relevance) to diagnostically-useful, EIT-based measures. With a systems-level perspective, we hope to help clarify how various components of an EIT system relate to each other and to the eventual diagnostic value.

In the opinion of the authors, EIT is at a time of transition. For many of its applications, EIT is reliable and reproducible [7], [42]. The important question is whether it is relevant, in the sense that EIT-based measures can be useful to manage

patients and improve outcomes. To be successful, EIT must provide new clinically-relevant information which cannot be obtained, safely or conveniently, in another way. We feel the capabilities of EIT mean it is best seen as *monitoring++* (i.e. an improved monitoring technology), rather than *imaging−−* (i.e. a low-resolution imaging technology). Using its high temporal resolution, there are rich possibilities to explore novel fEIT modalities to extract specific physiological information.

To achieve this, we recommend a focus on: 1) *availability* of EIT software (for modeling, algorithm comparison, and reuse) as well as reference data; 2) *availability* of EIT devices (for phantom, animal and clinical use) as well as reference data; 3) *standards* for access to EIT data and images (such as a DICOM class); 4) robustness against electrode contact errors and interference (automatic compensation being the most important technical requirement); 5) *useful software* with an intuitive interface for the clinical and experimental user, which provides relevant parameters and calibrated units; 6) *standardized procedures* for EIT measurements indicating the required protocols for EIT and additional measures (e.g. ECG, pressure) and analysis approaches; 7) *clinically-motivated EIT research* based on collaborations focused on answering specific questions. To help further these goals, all software to create the figures in this paper is available at *eidors.org/eit-review2017*.

IV. Conclusion

EIT images internal electrical properties using body-surface measurements; it has high temporal but low spatial resolution, and has the advantage of being non-invasive and potentially low cost. It offers exciting possibilities for imaging and functional monitoring in several applications, and is currently seeing clinical use for ventilation monitoring. In this paper, we have reviewed the applications of EIT with the goal to elucidate the process of image interpretation, by elaborating each of the processes though which potentially diagnostically-relevant measures are determined from the underlying tissue properties.

References

[1] M Abboud *et al*; "Monitoring of peripheral edema using electrical bioimpedance measurements" *Conf IEEE EMBS* pp 641–642, 1995.

[2] A Adler, R Guardo, Y Berthiaume. "Impedance imaging of lung ventilation: do we need to account for chest expansion?" *IEEE T Biomed Eng*, 43:414–420, 1996.

[3] A Adler, WRB Lionheart "Uses and abuses of EIDORS: An extensible software base for EIT" *Physiol Meas* 27:S25–S42, 2006.

[4] A Adler *et al*; "GREIT: a unified approach to 2D linear EIT reconstruction of lung images" *Physiol Meas*, 30:S35–S55, 2009

[5] A Adler *et al*; "Cerebral perfusion imaging using EIT", *Proc EIT 2017*, p.43, Dartmouth, NH, USA, June 21–24, 2017

[6] A Adler, PO Gaggero, Y Maimaitijiang, "Adjacent Stimulation and Measurement Patterns Considered Harmful" *Physiol Meas*, 32:731–744, 2011.

[7] A Adler *et al*; "Whither lung EIT: where are we, where do we want to go, and what do we need to get there?" *Physiol Meas*, 33:679–694, 2012.

[8] A Adler, B Grychtol, R Bayford "Why is EIT so hard, and what are we doing about it?" *Physiol Meas*, 36:1067–1074. 2015.

[9] A Adler, WRB Lionheart, "Conductivity perturbations in EIT" *Proc. Conf. EIT2016*, p 26, Neuchâtel, Switzerland, Jun 2–5, 2015.

[10] A Adler, R Gaburro, WRB Lionheart, "Electrical Impedance Tomography", in *Handbook of Mathematical Methods in Imaging*, 2nd ed O Scherzer (Ed), Springer, 2016.

[11] A Adler, A Boyle, WRB Lionheart "Efficient computations of the Jacobian matrix using different approaches are equivalent" *Proc. Conf. EIT2017*, p.74 Dartmouth, USA, Jun 21–24, 2017.

[12] LA Allaud, MH Martin; "Schlumberger, the history of a technique", John Wiley and Sons, New York. 1977.

[13] KY Aristovich *et al*; "A method for reconstructing tomographic images of evoked neural activity with electrical impedance tomography using intracranial planar arrays", *Physiol meas*. 35:1095–1110, 2014.

[14] M Assenheimer *et al*; "The T-SCAN technology: electrical impedance as a diagnostic tool for breast cancer detection." *Physiol Meas* 22:1–8, 2001.

[15] DC Barber, BH Brown, IL Freeston; "Imaging Spatial distributions of resistivity using Applied Potential Tomography". *Electronics Letters* 19:93–95, 1983.

[16] RH Bayford; "Bioimpedance tomography (electrical impedance tomography)" *Ann Rev Biomed Eng* 8:63–91, 2006.

[17] MS Beck, RA Williams, "Process tomography: a European innovation and its applications" *Meas Sci Technol* 7:215–224, 1996

[18] M Bodenstein, M David, K Markstaller; "Principles of electrical impedance tomography and its clinical application." *Crit Care Med* 37:713–24, 2009.

[19] L Borcea; "Electrical impedance tomography." *Inverse Prob* 18:R99–R136, 2002.

[20] A Borsic, WR Lionheart, CN McLeod CN, "Generation of anisotropic-smoothness regularization filters for EIT. IEEE transactions on medical imaging." 21:579-587, 2002.

[21] A Borsic *et al*; "Sensitivity study and optimization of a 3D electric impedance tomography prostate probe" *Physiol Meas* 30:S1–S19, 2009.

[22] A Borsic, A Adler, "A primal dual-interior point framework for using the L1-norm or the L2-norm on the data and regularization terms of inverse problems" *Inverse Prob*, 28:095011, 2012.

[23] A Boyle, A Borsic, A Adler, "Addressing the computational cost of large EIT solutions" *Physiol Meas* 33:787–800, 2012.

[24] F Braun *et al*; "A Versatile Noise Performance Metric for Electrical Impedance Tomography Algorithms" In press *IEEE T Biomed Eng* DOI:10.1109/TBME.2017.2659540

[25] BH Brown, AD Seagar, "The Sheffield data collection system", *Clin Phys Physiol Meas*, 8(Suppl A): 91–97, 1987.

[26] BH Brown; "Electrical impedance tomography (EIT): a review." *J Med Eng Technol* 27:97–108, 2003.

[27] AP Calderón, "On an inverse boundary value problem", in *Seminar on Numerical Analysis and its Applications to Continuum Physics*, Rio de Janeiro, Editors W.H. Meyer and M.A. Raupp, Sociedade Brasileira de Matematica, pp 65–73, 1980.

[28] M Cheney *et al*; "NOSER: An algorithm for solving the inverse conductivity problem" *Int J Imag Syst Technol* 2:66–75, 1990.

[29] M Cheney, D Isaacson, JC Newell; "Electrical Impedance Tomography", SIAM Review, 41:85–101, 1999.

[30] KS Cheng *et al*; "Electrode models for electric current computed tomography", *IEEE T Biomed Eng* 36:918-924, 1989.

[31] V Cherepenin *et al*; "A 3D electrical impedance tomography (EIT) system for breast cancer detection." *Physiol Meas* 22:9–18, 2001.

[32] MH Choi *et al*; "A reconstruction algorithm for breast cancer imaging with electrical impedance tomography in mammography geometry." *IEEE T Biomed Eng* 54:700-10, 2007.

[33] EL Costa, RG Lima, MB Amato MB; "Electrical impedance tomography." *Curr Opin Crit Care* 15:18–24, 2009.

[34] EL Costa *et al*; "Bedside estimation of recruitable alveolar collapse and hyperdistension by electrical impedance tomography." *Int Care Med* 35:1132–1137, 2009.

[35] N Coulombe *et al*; "A parametric model of the relationship between EIT and total lung volume." *Physiol Meas* 26:401–411, 2005.

[36] AM Dijkstra *et al*; "Review clinical applications of electrical impedance tomography" *J Medical Eng Technol*, 17:89–98, 1993.

[37] D Ferrario *et al*; "Toward morphological thoracic EIT: major signal sources correspond to respective organ locations in CT" *IEEE T Biomed Eng* 59:3000–3008, 2012.

[38] I Frerichs; "Electrical impedance tomography (EIT) in applications related to lung and ventilation: a review of experimental and clinical activities." *Physiol Meas* 21:R1–R21, 2000.

[39] I Frerichs *et al*; "Regional lung perfusion as determined by electrical impedance tomography in comparison with electron beam CT imaging" *IEEE T Med Imag* 21:646–652, 2002.

[40] I Frerichs *et al*; "Electrical Impedance Tomography – a method for

monitoring regional lung aeration and tidal volume distribution?", *Int Care Med* 29:2312–2316, 2003.
[41] I Frerichs, T Becher, N Weiler; "Electrical impedance tomography imaging of the cardiopulmonary system." *Curr Opin Crit Care* 20:323–32, 2014.
[42] I Frerichs *et al*; "Chest electrical impedance tomography examination, data analysis, terminology, clinical use and recommendations: consensus statement of the TRanslational EIT developmeNt stuDy group" *Thorax*, 72:83–93, 2017.
[43] S Gabriel, RW Lau, C Gabriel, "The dielectric properties of biological tissues: III. Parametric models for the dielectric spectrum of tissues", *Phys Med Biol* 41:2271–2293, 1996.
[44] C Gabriel, A Peyman, EH Grant, *Electrical conductivity of tissue at frequencies below 1 MHz Phys Med Biol* 54:4863–4878, 2009.
[45] DB Geselowitz, "An application of electrocardiographic lead theory to impedance plethysmography" *IEEE T Biomed Eng* 1:38–41, 1971.
[46] C Gómez-Laberge, JH Arnold, GK Wolf "A Unified Approach for EIT Imaging of Regional Overdistension and Atelectasis in Acute Lung Injury", *IEEE T Medical Imag*, 31:834–842, 2012.
[47] B Grychtol *et al*; "Impact of model shape mismatch on reconstruction quality in Electrical Impedance Tomography" *IEEE T Medical Imag*, 31:1754–1760, 2012.
[48] B Grychtol, A Adler, "FEM electrode refinement for Electrical Impedance Tomography" *Conf IEEE EMBS* pp 6429–6432, 2013.
[49] B Grychtol *et al*; "Functional Validation and Comparison Framework for EIT Lung Imaging" *PLoS ONE* 9:e103045, 2014.
[50] B Grychtol, B Müller, A Adler, "3D EIT image reconstruction with GREIT", *Physiol Meas* 37:785–800, 2016.
[51] RJ Halter *et al*; "Electrical impedance spectroscopy of the human prostate." *IEEE T Biomed Eng* 54:1321-7, 2007.
[52] G Hahn *et al*; "Changes in the thoracic impedance distribution under different ventilatory conditions", *Physiol Meas* 16:A161–173, 1995.
[53] AE Hartinger, H Gagnon, R Guardo, "Accounting for hardware imperfections in EIT image reconstruction algorithms" *Physiol Meas* 28:S13–S27,2007
[54] RP Henderson, JG Webster; "An Impedance Camera for Spatially Specific Measurements of the Thorax" *IEEE T Biomed Eng* 25:250–254, 1978.
[55] CN Herrera *et al*; "Direct 2-D reconstructions of conductivity and permittivity from EIT data on a human chest." *IEEE T Med Imag*, 34:267–74, 2015.
[56] AE Hoetink *et al*; "On the flow dependency of the electrical conductivity of blood" *IEEE T Biomed Eng* 51:1251–1261, 2004.
[57] DS Holder, "Electrical impedance tomography with cortical or scalp electrodes during global cerebral ischaemia in the anaesthetised rat." *Clin Phys Physiol Meas* 13:87–98, 1992.
[58] DS Holder, ed; "Electrical impedance tomography: methods, history and applications." CRC Press, 2004.
[59] P Hua *et al*; "Iterative reconstruction methods using regularization and optimal current patterns in electrical impedance tomography" *IEEE T Med Imag* 10:621–628, 1991.
[60] IEC 60601-1:2015, "Medical Electrical Equipment Part 1: General Requirements for Basic Safety and Essential Performance", Brussels: International Electrotechnical Commission, 2015
[61] D Goble, D Isaacson. "Optimal current patterns for three-dimensional electric current computed tomography" *Conf. IEEE EMBS* pp 463–464, 1989.
[62] D Isaacson; "Distinguishability of conductivities by electric current computed tomography." *IEEE T Med Imag* 5: 91–95, 1986.
[63] J Jossinet, "The impedivity of freshly excised human breast tissue" *Physiol Meas* 19:61–75, 1998.
[64] S Khan *et al*; "FPGA-based voltage and current dual drive system for high frame rate electrical impedance tomography" *IEEE T Medical Imag*, 34:888–901, 2015.
[65] J Larsson, "Electromagnetics from a quasistatic perspective", *Am J Physics* 75:230-239, 2007.
[66] S Leonhardt *et al*; "Electric impedance tomography for monitoring volume and size of the urinary bladder." *Biomedizinische Technik* 56:301–307, 2011
[67] S Leonhardt, B Lachmann; "Electrical impedance tomography: the holy grail of ventilation and perfusion monitoring?" *Int Care Med* 38:1917-1929, 2012.
[68] JH Li, C Joppek, U Faust, "Fast EIT data acquisition system with active electrodes and its application to cardiac imaging" *Physiol Meas*. 17:A25–A32, 1996.
[69] JM Lee, G Uhlmann, "Determining anisotropic real-analytic conductivities by boundary measurements," *Comm. Pure Appl. Math.* 42:1097–1112, 1989.
[70] WRB Lionheart, J Kaipio, CN McLeod; "Generalized optimal current patterns and electrical safety in EIT." *Physiol Meas* 22: 85–90, 2001.
[71] WRB Lionheart, K Paridis, "Finite elements and anisotropic EIT reconstruction" *J Phys: Conf Ser* 224:012022, 2010.
[72] HA Lorentz, "The theorem of Poynting concerning the energy in the electromagnetic field and two general propositions concerning the propagation of light" *Amsterdammer Akademie der Wetenschappen* 4:176–187, 1896.
[73] Lozano A, Rosell J, Pallas-Areny R. "Errors in prolonged electrical impedance measurements due to electrode repositioning and postural changes." *Physiol Meas* 16:121–130, 1995.
[74] S Lundin, O Stenqvist; "Electrical impedance tomography: potentials and pitfalls." *Curr Opin Crit Care* 18:35–41, 2012.
[75] Y Mamatjan *et al*; "Evaluation and Real-Time Monitoring of Data Quality in Electrical Impedance Tomography". *IEEE T Med Imaging* 32:1997–2005, 2013.
[76] YF Mangnall *et al*; "Applied potential tomography: a new noninvasive technique for assessing gastric function", *Clin Phys Physiol Meas*, 8:119-129 1987.
[77] P Metherall *et al*; "Three dimensional electrical impedance tomography" *Nature* 380:509-512, 1996.
[78] JC Newell *et al*; "Assessment of acute pulmonary edema in dogs by electrical impedance imaging." *IEEE T Biomed Eng* 43:133–138, 1996.
[79] DT Nguyen *et al*; "A review on electrical impedance tomography for pulmonary perfusion imaging." *Physiol Meas* 33:695–706, 2012.
[80] A Nissinen *et al*; "Compensation of errors due to discretization, domain truncation and unknown contact impedances in electrical impedance tomography" *Meas Sci Technol*. 20:105504, 2009.
[81] B Packham *et al*; "Comparison of frequency difference reconstruction algorithms for the detection of acute stroke using EIT in a realistic head-shaped tank" *Physiol Meas* 33:767–786, 2012.
[82] N Polydorides, WRB Lionheart. "A Matlab toolkit for three-dimensional electrical impedance tomography: a contribution to the Electrical Impedance and Diffuse Optical Reconstruction Software project." *Meas Sci Technol* 13:1871–1883, 2002.
[83] M Proença *et al*; "Influence of heart motion on cardiac output estimation by means of electrical impedance tomography: a case study" *Physio. Meas*, 36:1175–1192, 2015.
[84] M Proença *et al*; "Non-invasive monitoring of pulmonary artery pressure from timing information by EIT: experimental evaluation during induced hypoxia" *Physiol Meas* 37:713–726, 2016.
[85] S Pulletz *et al*; "Regional lung opening and closing pressures in patients with acute lung injurys", *J Critical Care*, 27:3:323.e11–323.e18, 2012.
[86] S Pulletz *et al*; "Dynamics of regional lung aeration determined by electrical impedance tomography in patients with acute respiratory distress syndrome", *Multidiscip Respir Med* 7:44, 2012.
[87] M Rapin *et al*; "Cooperative sensors: a new approach towards wearable EIT systems", *Proc. Conf. EIT2016*, p 44, Neuchâtel, Switzerland, Jun 2–5, 2015.
[88] T Riedel, I Frerichs; "Electrical impedance tomography." *Eur Respir Mon* 47:195–205, 2010.
[89] A Romsauerova *et al*; "Multi-frequency electrical impedance tomography (EIT) of the adult human head: initial findings in brain tumours, arteriovenous malformations and chronic stroke, development of an analysis method and calibration." *Physiol Meas* 27:S146–S161, 2006.
[90] CJ Roth *et al*; "Physiological Measurement Correlation between alveolar ventilation and electrical properties of lung parenchyma" *Physiol Meas* 36: 1211–1226, 2015
[91] RJ Sadleir *et al*; "Detection of intraventricular blood using EIT in a neonatal piglet model." *Conf IEEE EMBS* pp 3169-3172, 2009.
[92] TF Schuessler, JHT Bates, "Utility of an esophageal reference electrode for thoracic electrical impedance tomography" *Conf. IEEE EMBS* pp 559–560, 1995
[93] KJ Seo *et al*; "Frequency-difference electrical impedance tomography (fdEIT): algorithm development and feasibility study", *Physiol Meas* 29:929–944, 2008.
[94] D Silvera-Tawil *et al*; Electrical Impedance Tomography for Artificial Sensitive Robotic Skin: A Review *IEEE Sensors J*, 15:2001–2016, 2015.
[95] HJ Smit *et al*; "Electrical impedance tomography to measure pulmonary perfusion: Is the reproducibility high enough for clinical practice?" *Physiol Meas* 24:491-499, 2003.
[96] J Solà *et al*; "Non-invasive monitoring of central blood pressure by Electrical Impedance Tomography (EIT): first experimental evidence" *Med Biol Eng Comput*, 49:409–415, 2011.
[97] Soleimani M, "Electrical impedance tomography imaging using a priori ultrasound data." *Biomedical engineering online* 5, 2006.

DOI:10.1186/1475-925X-5-8
[98] M Soleimani, C Gómez-Laberge, A Adler. "Imaging of conductivity changes and electrode movement in EIT", *Physiol Meas* 27:S103–S113, 2006.
[99] E Somersalo *et al*; "Layer stripping: a direct numerical method for impedance imaging." *Inverse Prob* 7:899–926, 1991.
[100] J Sylvester, G Uhlmann, "A uniqueness theorem for an inverse boundary value problem n electrical prospection" *Comm Pure Appl Math* 3991-3112, 1986.
[101] A Tamburrino, G Rubinacci, "A new non-iterative in version method in electrical resistance tomography", *Inverse Prob*, 18:1809-1829, 2002.
[102] CJC Trepte *et al*; "Electrical impedance tomography (EIT) for quantification of pulmonary edema in acute lung injury", *Crit Care*, 20:18, 2016.
[103] CJC Trepte *et al*; "Electrical impedance tomography (EIT) for non-invasive assessment of stroke volume variation in health and experimental lung injury" *Br J Anaesthesia*, 118:68–76, 2017.
[104] G Uhlmann; "Electrical impedance tomography and Calderón's problem." *Inverse Prob*.25:123011, 2009.
[105] B Vogt *et al*; "Heterogeneity of regional ventilation in lung-healthy adults", *Proc. Conf. EIT2016*, p.106, Stockholm, Sweden, Jun 19–23, 2016.
[106] A Vonk-Noordegraaf *et al*; "Determination of stroke volume by means of electrical impedance tomography" *Physiol Meas* 21:285–293, 2000
[107] AD Waldmann *et al*; "Assessment of silent spaces at different PEEP levels by electrical impedance tomography in severe COPD". *Int Care Med Experimental* 3:A456, 2015.
[108] AD Waldmann *et al*; "Performance of novel patient interface for electrical impedance tomography applications" In press: *J Medical Biol Eng*, 2017.
[109] Y Wan *et al*; "Transrectal electrical impedance tomography of the prostate: Spatially coregistered pathological findings for prostate cancer detection" *Medical physics* 40:063102, 2013.
[110] GK Wolf *et al*; "Mechanical ventilation guided by electrical impedance tomography in experimental acute lung injury." *Crit Care Med* 41:1296-304, 2013.
[111] TJ Yorkey, JG Webster, WJ Tompkins, "Comparing reconstruction algorithms for electrical impedance tomography" *IEEE T Biomed Eng* 11:843–852, 1987.